Modeling enamel matrix secretion in mammalian teeth

Teemu J. Häkkinen[1,2,*], S. Susanna Sova[1,3], Ian J. Corfe[1], Leo Tjäderhane[4], Antti Hannukainen[2] & Jukka Jernvall[1,*]

[1]Developmental Biology Program, Institute of Biotechnology, University of Helsinki, P.O. Box 56, FI-00014 Helsinki, Finland.

[2]Department of Mathematics and Systems Analysis, Aalto University, P.O. Box 11100, FI-00076 Aalto, Finland.

[3]Department of Geosciences and Geography, University of Helsinki, P.O. Box 64, FI-00014 Helsinki, Finland.

[4]Department of Oral and Maxillofacial Diseases, Helsinki University Hospital, University of Helsinki, P.O. Box 41, FI-00014, Helsinki, Finland.

[*]To whom correspondence should be addressed: Email: hakkinen@fastmail.com or jernvall@fastmail.fm

Author Contributions: T.J.H., S.S.S. and J.J. conceived the study, T.J.H. constructed the model, A. H. suggested the velocity extension scheme and provided input on the algorithms, S.S.S., I.J.C. and L.T. collected and processed the empirical data, T.J.H., S.S.S. and J.J. performed the simulations, analyzed the results and wrote the paper. All authors discussed the results and provided input and scientific interpretations on the manuscript.

Abstract

The most mineralized tissue of the mammalian body is tooth enamel. Especially in species with thick enamel, three-dimensional (3D) tomography data has shown that the distribution of enamel varies across the occlusal surface of the tooth crown. Differences in enamel thickness among species and within the tooth crown have been used to examine taxonomic affiliations, life history, and functional properties of teeth. Before becoming fully mineralized, enamel matrix is secreted on the top of a dentine template, and it remains to be explored how matrix thickness is spatially regulated. To provide a predictive framework to examine enamel distribution, we introduce a computational model of enamel matrix secretion that maps the dentine topography to the enamel surface topography. Starting from empirical enamel-dentine junctions, enamel matrix deposition is modeled as a diffusion-limited free boundary problem. Using laboratory microCT and synchrotron tomographic data of pig molars that have markedly different dentine and enamel surface topographies, we show how diffusion-limited matrix deposition accounts for both the process of matrix secretion and the final enamel distribution. Simulations reveal how concave and convex dentine features have distinct effects on enamel surface, thereby explaining why the enamel surface is not a straightforward extrapolation of the dentine template. Human molar simulations show that even subtle variation in dentine topography can be mapped to the enamel surface features. Mechanistic models of extracellular matrix deposition can be used to predict occlusal morphologies of teeth.

Introduction

Most mammalian species have their teeth covered by a layer of highly mineralized enamel. The thickness of the enamel layer relative to the tooth size ranges from thin to very thick. These differences among species, and also increasingly within the tooth crown, have been informative in studies focused on functional properties of teeth, taxonomy, and life history (1-9). Even though mutations in genes required for enamel matrix secretion and maturation are known to affect the enamel thickness in mammals (10), relatively little is known about the regulatory changes that might underlie the variation in enamel thickness among populations or species

(1,11,12). Even less is known about the regulation of enamel thickness variation within the tooth crown, which contrasts with the increasing availability of 3D tomography data on various species. Analyses of such tomography data show that even though the enamel surface topography reflects the enamel-dentine junction (EDJ) topography, the enamel surface is not a simple extrapolation of the EDJ shape (13-15). Because enamel distribution is not developmentally remodeled after formation, and because the internal structure of mineralized enamel retains developmental information, tomography data of fully formed teeth can be used to examine mechanisms underlying variation in enamel thickness. To provide mechanistic insights into the regulation of enamel thickness, here we combine tomography data on enamel distribution with a computational approach and introduce a model to simulate enamel matrix secretion.

Results

The Model Principles and Simulation of Artificial Shapes. The enamel matrix is secreted by specialized epithelial cells, the ameloblasts, which depart from the EDJ. The EDJ is defined by the mesenchymal dentine matrix, whose secretion begins first (Fig. 1A). For empirical tests, we used EDJs of real teeth as the starting point to simulate matrix secretion (Fig. 1A). Matrix deposition is modeled as a diffusion-limited free boundary problem, motivated by the classical Stefan problem that models phase transition of undercooled liquid by assuming that the rate of phase transition from liquid to solid is limited by a diffusion process (see Methods and Supplementary Information) (16,17). Here we similarly assume that the growth of the matrix front is a diffusion-limited process: The advancement of the ameloblast layer departing from the EDJ is assumed to be limited by the diffusion of nutrition, by which we refer communally to all the factors that ameloblasts require for the secretion of the matrix (Fig. 1B). The model

parameters adjust the nutrition diffusion rate, the amount of nutrition required for growth, and the interfacial tension or stiffness of the advancing ameloblast layer (Methods). Model equations are solved using the finite element method, and the matrix interface (the ameloblast layer) is tracked using the level set method (Supplementary Information). The source code of the Matlab implementation of the model is freely available (Methods). For computational efficiency, the model is implemented in 2D and 3D reconstructions are obtained by simulating multiple sections that are combined into volumes.

The fundamental component of the model is the assumption that the growth of the matrix requires a net influx of a diffusing nutrient substance. At the initial stage nutrition is assumed to be present exterior to the dentine, and the nutrient is also replenished by a constant background source (Methods). By controlling the relative amount of background production, we examine two hypothetical matrix secretion processes. The primary process tested is a diffusion-limited secretion in which concave surfaces are progressively exaggerated as the features protruding into the nutrition-rich domain receive more nutrition than the concavities (Fig. 1C). An alternative process assumes excess availability of nutrition through strong background production, leading to a moving boundary of uniform thickness (Fig. 1D). This latter process in fact closely approximates a simple geometric extrapolation of matrix thickness from the EDJ, which we use as a null hypothesis to demonstrate the non-linearity of the matrix deposition. Simulations of matrix secretion using a synthetic EDJ shape show that whereas convex EDJ surfaces result in relatively linear extrapolation of the enamel surface in both simulations (Fig. 1C, D), concave surfaces of diffusion-limited simulations behave nonlinearly (Fig. 1C). Additionally, reducing interfacial tension in the simulations increases small undulations in the moving front (Fig. 1E), suggesting that lowered stiffness of the ameloblast layer may underlie crenulated enamel found in taxa such as *Chiropotes* (saki monkeys) with relatively smooth EDJ (14).

Diffusion-Limited Simulations Predict Enamel Distribution on Pig Molar Teeth. To simulate enamel matrix secretion in real teeth, first we focused on domestic pig molar teeth that exhibit substantial variation in enamel thickness and EDJ topography (Figs 1A, 2A, ref. 18). EDJ and enamel surface shapes were reconstructed from microCT scans of first lower molars (Fig. 2A, Methods). From the data, horizontal slices of cusps were extracted (Fig. 2A) and the EDJs were used as the starting point for the simulations. The horizontal plane represents a relatively synchronous front of enamel matrix secretion and captures the complex EDJ morphology of the pig molars (18). The simulations show that the diffusion-limited process reproduces the deep narrow furrows or fissures present on the concave sides of the real cusps (Fig. 2A, B). In contrast, these features are lost when the enamel matrix is geometrically extrapolated from the EDJ, or when modeling with excess background nutrition (Fig. 2C). These results support the role of a diffusion-limited-like process in the regulation of enamel matrix secretion, and underscore the distinct effects that the convex and concave EDJ features impose on the enamel distribution. Indeed, whereas cusps of individual pigs vary in their detailed cusp morphology, the overall distribution of convex and concave features is conserved (Fig. S1).

Next we simulated the matrix secretion in a whole cusp with both convex and concave features (Methods). A 3D reconstruction of these simulations show that the diffusion-limited model captures the overall enamel thickness patterns in which concavities show reduced enamel thickness whereas ridges show increased enamel thickness (Fig. 3, Fig. S2). A small ridge present in the middle of a dentine concavity results in a local thickening of the enamel within an otherwise deep fissure (arrow heads in Fig. 3A-C), a feature completely lost in geometrically extrapolated surfaces (Fig. 3D).

Diffusion-Limited Simulations Reproduce the Progression of Matrix Secretion. In addition to the distribution of enamel in fully formed tooth, the diffusion-limited simulations can be used to examine the progression of the matrix secretion process itself. The successive positions of the matrix-secreting front during development is recorded in teeth by incremental lines (laminations or striae of Retzius, ref. 9) that are broadly analogous to growth rings in trees (19). These are preserved in mature enamel and can be observed from thin sections or through phase contrast synchrotron imaging (19,20). We obtained synchrotron data from a pig molar and compared the positions of individual incremental lines in convex cusp ridges with the lines in cusp concavities (Fig. 4A). Both the virtual incremental lines of diffusion-limited simulations and empirical incremental lines show initially relatively uniform distances from the EDJ, but this uniformity disappears and the differences between ridges and valleys become progressively larger as the secretion accelerates in the ridges and slows down in the valleys (Fig. 4). These results are suggestive that in addition to the final patterns of enamel distribution, the diffusion-limited model captures aspects of the actual secretion process.

Subtle EDJ Concavities Are Sufficient to Produce Complex Enamel Surface Features. Pigs are an example of species with relatively pointed molar cusps, allowing the simulation of matrix secretion in the horizontal plane. In contrast, molars of primates with thick enamel, including humans, typically have relatively low cusp relief. Therefore, to capture matrix secretion of human molar morphology, we run the diffusion-limited simulations vertically. Because the enamel becomes globally thinner towards the tooth neck, or lower portion of the tooth crown, we implemented a nutrient sink at the base (Methods). The sink decreases the rate of matrix formation towards the base of the crown, thereby approximating crown formation and the apical decline in matrix secretion before the initiation of root development (ref. 9, Fig. 5A). The

147 simulations show the subtle waviness of the human EDJ, with manly concave ripple-like
148 features, is enough to produce the characteristic undulations of the enamel surface (Fig. 5B,C).
149 These features are further refined by simulations using lateral braces mimicking the presence of
150 adjacent teeth and alveolar bone (Fig. 5B), in agreement with the suggested role of the
151 surrounding tissues in the regulation of tooth shape and mineralization (21,22). Taken together,
152 these simulations indicate that even subtle EDJ features present in many hominids are important
153 for the functional surface morphology of the tooth.

154

155 **Conclusions**

156 Our diffusion-limited model suggests an objective basis for mapping the EDJ morphology to
157 enamel surface morphology. The simulations point to the critical role of convex and concave
158 EDJ surface features in the regulation of final tooth surface morphology. These results also
159 indicate that complex patterns of enamel thickness on a tooth crown can result from a single
160 developmental process, without the need to evoke specific control or explanations for individual
161 thickness features. Combined with in-depth analyses of enamel formation rates (4, 9, 18) and
162 isotope compositions (23, 24) obtainable from sections, our model should help to move studies
163 using enamel thickness towards more mechanistic and predictive science. This approach should
164 also be applicable to other systems with extracellular matrix secretion, or organs in which
165 directional tissue growth may be diffusion limited. Diffusion-limited free boundary problems
166 have a long history in mathematics (16, 17, 25), and as shown here, they can contribute to
167 solving biological problems.

168

169

Materials and Methods

Diffusion-limited model. We solve the model using a finite element method algorithm presented in ref. 26. For implementation details and source code, see Supplementary Information and https://github.com/tjhakkin/biomatrix.

Dental data and processing. Molars were extracted, stored and microCT imaged using the protocols, and pig and human molar samples described in ref. 18. The voxel resolutions were 10 to 24 µm (pig molars) and 17 µm (human molars), and downsampled to 44 µm (pig molars) and 66 µm (human molars). Synchrotron data was collected at beamline ID19 of the European Synchrotron Radiation Facility, with voxel resolution 2.24 µm, keV = 91, and 6000 projections in 4x accumulation mode. Synchrotron data reconstruction used Paganin style single propagation distance phase contrast. All the image processing steps after primary tomography reconstructions were carried out with Fiji 2.0 (27). To digitize EDJs for simulations, EDJs in each individual section were traced with a freehand selection, and the area was converted to a line (Edit/Selection/Area to Line). The line was then interpolated with an interval of 10 pixels (Edit/Selection/Interpolate), fitted to a spline (Edit/Selection/Fit spline), and adjusted manually to follow the EDJ if needed. The splines were saved in ROI Manager (Analyze/Tools/ROI manager/more/save). The splines were saved as XY coordinates (File/Save As/XY Coordinates) that were converted to level sets using a Python script, included with the source code. During the conversion the spatial node density and the relative size of the EDJ within the domain were also defined. To scale different sized EDJs uniformly (e.g., when EDJs become smaller towards the cusp tip), two small triangles placed in diagonally opposing corners were included in each level set conversion. To enhance the visualization of the incremental lines in synchrotron reconstructions, three adjacent slices were averaged.

Simulations and analyses. The main simulation parameters are listed in Table S1. Simulation output for each step is an image file. The pig trigonids and talonids were simulated separately

(Fig. 2B). To compensate for the isolated entoconid cusp being larger (Fig. 3) than when part of the talonid (Fig. 2), interfacial tension and number of iterations were decreased in the individual cusp simulations. For simulations of multiple sections (Figs 3, 5C), all the sections of the analyzed step were merged into a stack in Fiji. For the pig molar cusp (Fig. 3), every second microCT slice (20 µm interval, 51 slices), and for the human molar (Fig. 5C), every fifth slice (66 µm interval, 27 slices) was simulated. We used the basal sink to approximate developmental progression in the vertical simulations. Because intercuspal regions lack the sink, vertical simulations slightly exaggerate enamel thickness in valleys relative to cusp tips. Geometric extrapolation of enamel thickness was obtained in Fiji by fitting a fixed sized circle along the EDJ (Process/Morphology/Gray Morphology/Dilate). To visualize enamel thickness in 3D, the EDJ and enamel surfaces were exported from Fiji (surfaces exported as Wavefront .obj from 3D Viewer plugin) and imported into Meshlab (http://meshlab.sourceforge.net/). In Meshlab, Hausdorff distance was used to compare distances between two surfaces (28). The distances were calculated after smoothing the meshes with Laplacian smooth (3 steps). All 3D visualizations use orthographic projections.

Acknowledgements

We thank H. Suhonen for help with microCT imaging, and J. Laakkonen for help with material. We acknowledge the European Synchrotron Radiation Facility for provision of synchrotron radiation facilities and thank P. Tafforeau for assistance in using beamline ID19. We thank M. Fortelius and the members of the Center of Excellence in Experimental and Computational Developmental Biology Research for discussions or advise. Financial support was provided by the Academy of Finland and Vilho, Yrjö and Kalle Väisälä Foundation.

References

1. Schwartz GT (2000) Taxonomic and functional aspects of the patterning of enamel thickness distribution in extant large-bodied hominoids. *Am J Phys Anthropol* 111:221–244.

2. Grine FE (2005) Enamel Thickness of Deciduous and Permanent Molars in Modern *Homo sapiens*. *Am J Phys Anthropol* 126:14–31.

3. Smith TM, Olejniczak AJ, Martin LB, Reid DJ (2005) Variation in hominoid molar enamel thickness. *J Hum Evol* 48:575–592.

4. Dean MC (2006) Tooth microstructure tracks the pace of human life-history evolution. *Proc R Soc B* 273:2799–2808.

5. Lucas P, Constantino P, Wood B, Lawn B (2008) Dental enamel as a dietary indicator in mammals. *BioEssays* 30:374–385.

6. Olejniczak AJ, Smith TM, Skinner MM, Grine FE, Feeney RNM, Thackeray JF, Hublin J-J (2008) Three-dimensional molar enamel distribution and thickness in Australopithecus and Paranthropus. *Biol Lett* 4:406–410.

7. Skinner MM, Alemseged Z, Gaunitz C, Hublin J-J (2015) Enamel thickness trends in Plio-Pleistocene hominin mandibular molars. *J Hum Evol* 85:35–45.

8 Pan L, Dumoncel J, de Beer F, Hoffman J, Thackeray JF, Duployer B, Tenailleau C, Braga J (2016) Further morphological evidence on South African earliest Homo lower postcanine dentition: Enamel thickness and enamel dentine junction. *J Hum Evol* 96:82–96.

9. Kierdorf H, Breuer F, Witzel C, Kierdorf U (2018) Pig enamel revisited – Incremental markings in enamel of wild boars and domestic pigs. *J Struc Biol*. doi: 10.1016/j.jsb.2018.11.009.

10. Wright JT, Hart TC, Hart PS, Simmons D, Suggs C, Daley B, Simmer J, Hu J, Bartlett JD, Li Y, Yuan Z A, Seow WK, Gibson CW (2009) Human and mouse enamel phenotypes resulting from mutation or altered expression of AMEL, ENAM, MMP20 and KLK4. *Cells Tissues Organs* 189:224–229.

11. Horvath JE, Ramachandran GL, Fedrigo O, Nielsen WJ, Babbitt CC, St. Clair EM, Pfefferle LW, Jernvall J, Wray GA, Wall CE (2014) Genetic comparisons yield insight into

248 the evolution of enamel thickness during human evolution. *J Hum Evol* 73:75–87.

249 12. Daubert DM, Kelley JL, Udod YG, Habor C, Kleist CG, Furman IK, Tikonov IN, Swanson
250 WJ, Roberts FA (2016) Human enamel thickness and ENAM polymorphism. *Int J Oral Sci*
251 8:93–97.

252 13. Skinner MM, Wood BA, Hublin J-J (2009) Protostylid expression at the enamel-dentine
253 junction and enamel surface of mandibular molars of *Paranthropus robustus* and
254 *Australopithecus africanus*. *J Hum Evol* 56:76–85.

255 14. Skinner MM, Evans A, Smith T, Jernvall J, Tafforeau P, Kupczik K, Olejniczak AJ, Rosas
256 A, Radovcic J, Thakeray JF, Toussaint M, Hublin J-J (2010) Contributions of enamel-
257 dentine junction shape and enamel deposition to primate molar crown complexity. *Am J*
258 *Phys Anthropol* 142:157–163.

259 15. Guy F, Lazzari V, Gilissen E, Thiery G (2015) To what extent is primate second molar
260 enamel occlusal morphology shaped by the enamel-dentine junction? *PLoS ONE*
261 10:e0138802. doi:10.1371/journal.pone.0138802.

262 16. Chen S, Merriman B, Osher S, Smereka PA (1997) A simple level set method for solving
263 Stefan problems. *J Comp Physics* 135:8–29.

264 17. Chen H, Min C, Gibou F (2009) A numerical scheme for the Stefan problem on adaptive
265 Cartesian grids with supralinear convergence rate. *J Com. Physics* 228:5803–5818.

266 18. Sova SS, Tjäderhane L, Heikkilä PA, Jernvall J (2018) A microCT study of three-
267 dimensional patterns of biomineralization in pig molars. *Front Physiol* 9:71 doi:
268 10.3389/fphys.2018.00071.

269 19. Beynon AD, Dean MC, Reid DJ (1991) On thick and thin enamel in Hominoids. *Am J Phys*
270 *Anthropol* 86:295–309.

271 20. Tafforeau P, Smith TM. (2008) Nondestructive imaging of hominoid dental microstructure
272 using phase contrast X-ray synchrotron microtomography. *J Hum Evol* 54:272–278.

273 21. Marchiori DF, Packota GV, Boughner JC (2016) Third-molar mineralization as a function
274 of available retromolar space. *Acta Odont Scan* 74:509–517.

275 22. Renvoisé E, Kavanagh, KD, Lazzari V, Häkkinen TJ, Rice R, Pantalacci S, Salazar-Ciudad

I, Jernvall J (2017) Mechanical constraint from growing jaw facilitates mammalian dental diversity. *Proc Nat Acad Sci, USA* 114:9403–9408.

23. Green DR, Oack G, Colman AS (2018) Determinants of blood water $\delta^{18}O$ variation in a population of experimental sheep: Implications for paleoclimate reconstruction. *Chem Geol* 485:32–43.

24. Smith TM, Austin C, Green DR Joannes-Boyau R, Bailey S, Dumitriu D Fallon S, Grün R, James HF, Moncel MH, Williams IS, Wood R, Arora M (2018) Wintertime stress, nursing, and lead exposure in Neanderthal children. *Sci Adv* 4:10:eaau9483.

25. Vuik C (1993) Some historical notes about the Stefan problem, *Nieuw Archief voor Wiskunde* 11:157–167.

26. Häkkinen T (2016) On Free Boundary Problems. MSc thesis, Aalto University (2016).

27. Schindelin J, Arganda-Carreras I, Frise E, Kaynig V, Longair M, Pietzsch T, Preibisch S, Rueden C, Saalfeld, S, Schmid B., Tinevez, JY, White DJ, Hartenstein V, Eliceiri K, Tomancak P, Cardona, A (2012) Fiji: an open-source platform for biological-image analysis. *Nat methods* 9:676–682.

28. Cignoni P, Rocchini C, Scopigno R (1998) Metro: measuring error on simplified surfaces *Comput Graph Forum* 17:167–174.

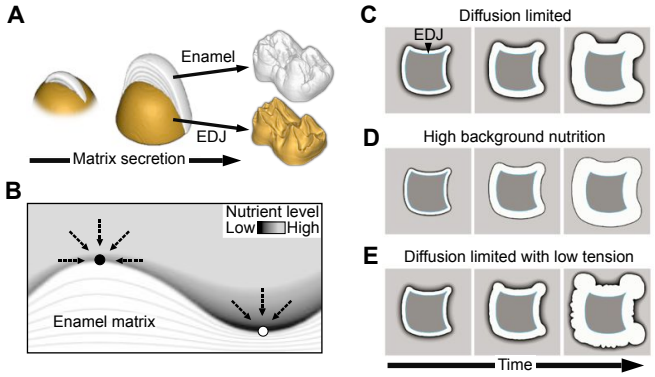

Figure 1. Modeling tooth enamel matrix secretion. (A) A schematic illustration of a cross section of enamel matrix being secreted on the top of dentine. In real teeth (a pig molar on the right), the enamel surface is not a linear representation of the dentine template (EDJ). (B) In a diffusion-limited model, differences in surface topography lead to ridges (black circle) receiving more nutrition (dashed arrows) than valleys (white circle). (C) Starting from a synthetic EDJ shape, diffusion-limited matrix deposition advances faster in convex than concave features. (D) Excess production of nutrition overcomes diffusion-limited effects and produces a uniform distribution of matrix. (E) Reducing surface tension of simulation in c results in crenulated matrix surface. For details of the model, see Methods, and parameters used in simulation are in Table S1.

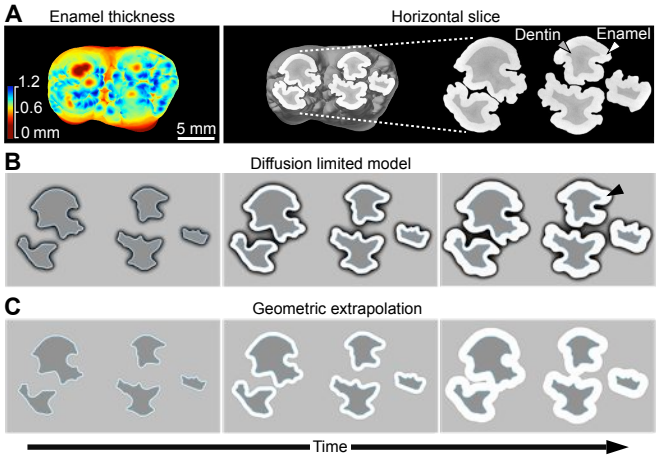

Figure 2. Diffusion-limited simulations approximate complex patterns of enamel thickness in the pig molar. (A) A heat map and a horizontal section of 3D tomography reconstruction of a pig molar shows the variable enamel thickness. (B) Using a horizontal EDJ section of a pig molar as an empirical template (A), diffusion-limited simulations of matrix secretion produce deep fissures present in concave surfaces. (C) Geometric extrapolation shows how the fissures are filled-in. In contrast, convex slopes are relatively similar between the simulations (B, C). All images show or are based on occlusal views of the left lower first molar. Simulations run until the lateral matrix thicknesses approximate the empirical enamel thicknesses, see Methods, and for parameters Table S1. Scale bar, 5 mm.

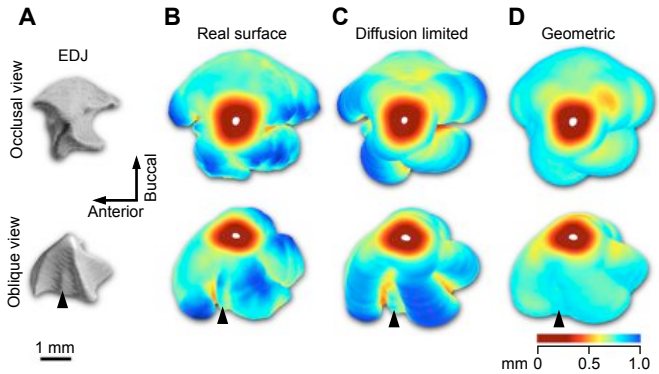

Figure 3. 3D distribution of enamel is predicted by the diffusion-limited model. (A) The EDJ of the pig entoconid cusp (arrowhead in Fig. 2B) has four ridges and only the buccal slope is convex whereas the other slopes are concave. (B) The enamel surface is thickest around the ridges and the EDJ concavities correspond to deep fissures with thinner enamel. The cusp tip with no EDJ has been removed from the 3D data. (C) The diffusion-limited matrix simulation, matched to have the enamel thickness of the convex lateral slope, captures the enamel distribution patterns of the pig cusp. The small ridge present in the mesial slope of the cusp (arrowhead in the oblique views) corresponds to a narrow ridge of matrix in the fissure both in the diffusion-limited simulation and the empirical enamel surface. (D) Geometric extrapolation from the EDJ results in relatively uniform 3D matrix thickness. The diffusion-limited simulations were done from 51 individual EDJ slices using the same parameter values (Table S1), and the geometric extrapolations from every slice. Enamel thickness measurements were done in 3D. The thinner enamel in the lower parts of the lingual cusp ridge of the real cusp (towards the bottom in occlusal view) is due to the vicinity of the adjacent hypoconid cusp, see Fig 2A,B. Scale bar, 1 mm.

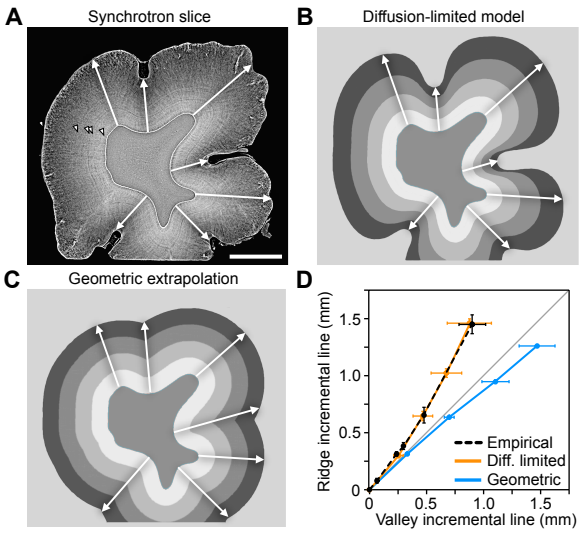

Figure 4. Incremental lines in pig molar tooth show comparable patterns to diffusion-limited matrix lines. (A) Incremental lines (arrowheads) are visible in a synchrotron imaged fully formed but unerupted cusp of the second lower molar. (B) Diffusion-limited simulation and (C) geometric extrapolation of matrix show contrasting patterns. The different shades of grey correspond to progressive steps in simulations (every fourth) and geometric extrapolation. (D) The arrows (in A,B,C) show the lines that are used to measure the progression of matrix secretion in the valleys (concave EDJ regions) and ridges (convex EDJ regions). Both the empirical and diffusion-limited simulations produce progressively thicker matrix in the ridges relative to the valleys (mean lines shown, error bars denote s.d.). The diffusion-limited simulation uses the same parameter values as the cusp in Fig 3. The border size (0.79) was set to produce the empirical enamel thickness using the same number of iterations as in Fig. 3. The target enamel thickness for the simulations was measured from the left side of the cusp. Because the cusp was physically trimmed for synchrotron imaging, the section is missing the lower side. Scale bar, 10 mm.

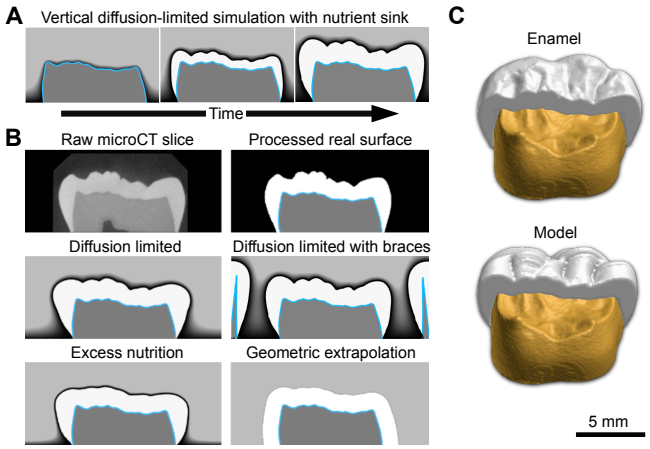

Figure 5. The subtle EDJ topography of human molars is sufficient to produce enamel surface features in diffusion-limited simulations. (A) To simulate the thick enamel of human molars that also have a low cusp relief, we combined vertically oriented simulations with a basal nutritional sink. The sink is used to simulate the shorter time of matrix secretion in the lower parts of the crown. (B) Diffusion-limited simulations reproduce the surface features that are lost in excess nutrition simulations and geometric extrapolations. Braces mimicking adjacent teeth and bone constrain lateral expansion of enamel matrix. (C) Obliquely lingual views of empirical and simulated enamel surfaces with a half of the EDJ (yellow) visible. The diffusion-limited simulations were done from 27 individual EDJ slices using the same parameter values (Table S1). The tooth shown is a human third lower molar. Scale bar, 5 mm.